Acoustic separation of circulating tumor cells

Peng Li[a], Zhangming Mao[a], Zhangli Peng[b,c], Lanlan Zhou[d,1], Yuchao Chen[a], Po-Hsun Huang[a], Cristina I. Truica[d], Joseph J. Drabick[d], Wafik S. El-Deiry[d,1], Ming Dao[b,2], Subra Suresh[e,2], and Tony Jun Huang[a,2]

[a]Department of Engineering Science and Mechanics, The Pennsylvania State University, University Park, PA 16802; [b]Department of Materials Science and Engineering, Massachusetts Institute of Technology, Cambridge, MA 02139; [c]Department of Aerospace and Mechanical Engineering, University of Notre Dame, Notre Dame, IN 46556; [d]Division of Hematology/Oncology, Penn State Hershey Cancer Institute, Hershey, PA 17033; and [e]Department of Biomedical Engineering and Department of Materials Science and Engineering, Carnegie Mellon University, Pittsburgh, PA 15213

Contributed by Subra Suresh, March 10, 2015 (sent for review February 5, 2015)

Circulating tumor cells (CTCs) are important targets for cancer biology studies. To further elucidate the role of CTCs in cancer metastasis and prognosis, effective methods for isolating extremely rare tumor cells from peripheral blood must be developed. Acoustic-based methods, which are known to preserve the integrity, functionality, and viability of biological cells using label-free and contact-free sorting, have thus far not been successfully developed to isolate rare CTCs using clinical samples from cancer patients owing to technical constraints, insufficient throughput, and lack of long-term device stability. In this work, we demonstrate the development of an acoustic-based microfluidic device that is capable of high-throughput separation of CTCs from peripheral blood samples obtained from cancer patients. Our method uses tilted-angle standing surface acoustic waves. Parametric numerical simulations were performed to design optimum device geometry, tilt angle, and cell throughput that is more than 20 times higher than previously possible for such devices. We first validated the capability of this device by successfully separating low concentrations (~100 cells/mL) of a variety of cancer cells from cell culture lines from WBCs with a recovery rate better than 83%. We then demonstrated the isolation of CTCs in blood samples obtained from patients with breast cancer. Our acoustic-based separation method thus offers the potential to serve as an invaluable supplemental tool in cancer research, diagnostics, drug efficacy assessment, and therapeutics owing to its excellent biocompatibility, simple design, and label-free automated operation while offering the capability to isolate rare CTCs in a viable state.

circulating cancer cells | cell separation | rare-cell sorting | acoustic tweezers | microfluidics

Circulating tumor cells (CTCs) serve as a liquid biopsy target for cancer diagnosis, genotyping, and prognosis (1). Monitoring the phenotypic and genotypic changes in CTCs during the course of chemotherapy treatment may be beneficial for guiding therapeutic decisions (2). In addition, they could provide new insights into the mostly elusive, yet deadly, process of cancer metastasis (3–5). To realize these potential benefits from CTCs, a better understanding of CTCs is needed. However, CTCs are difficult targets to probe owing to their extremely low concentration in peripheral blood (usually in the range of 1–100 cells/mL of blood). Therefore, effective cell separation methods are required to facilitate the study of CTCs.

Currently, CTC separation methods can be divided into two major categories: antibody-dependent or antibody-independent (4). Antibody-dependent methods use tumor-specific antibodies to identify CTCs. In this approach, in combination with magnetic or fluorescence markers, CTCs can be isolated from other blood cells (5, 6). The limitation of this strategy is that the separation of CTCs requires a priori knowledge of relevant antibodies. However, the expression of certain biomarkers is a highly dynamic and heterogeneous process that is specific to the patient. Thus, results obtained from antibody-dependent methods and the efficacy of these methods in detecting CTCs could be biased by the selection of the target antibodies.

As a complementary strategy, antibody-independent methods allow the separation of CTCs based on their physical properties, such as size, deformability, and electrical properties without the need to choose a priori the correct antibodies (7). Among the various separation methods that rely on cell physical properties (8–11), approaches predicated on acoustics offer several unique characteristics (12).

First, acoustic-based separation is known to offer excellent biocompatibility in terms of preserving the phenotype and genotype of the cell compared with other methods. Ultrasound, an acoustic method widely used in medical imaging for decades, has been proven to be extremely safe. Recent studies (13) also indicate that acoustic-based cell separation, which operates at a power intensity and frequency similar to ultrasonic imaging, has little impact on the viability, function, and gene expression of cells, under appropriate power intensities. Moreover, acoustic separation approaches do not require modification of the media in which cells are cultured and separated, and the cells do not require labeling or surface modification. This biocompatible separation process maximizes the potential of CTCs to be maintained at their native states, cultured, and analyzed in vitro or ex vivo. As a result, a large number of patient-derived cancer cells could be obtained through venipuncture instead of an invasive biopsy. These characteristics of the acoustic method enable not only a more accurate, comprehensive analysis of CTCs but also offer the potential for better cancer treatment options, such as noninvasive testing of drug susceptibility of cancer patients over the course of chemotherapy (3), and possible early detection of cancer and/or metastasis.

Second, acoustic-based cell separation is the only active separation method that can differentiate cells based on their size, density, compressibility, or a combination thereof. Using an

Significance

The separation and analysis of circulating tumor cells (CTCs) provides physicians a minimally invasive way to monitor the response of cancer patients to various treatments. Among the existing cell-separation methods, acoustic-based approaches provide significant potential to preserve the phenotypic and genotypic characteristics of sorted cells, owing to their safe, label-free, and contactless nature. In this work, we report the development of an acoustic-based device that successfully demonstrates the isolation of rare CTCs from the clinical blood samples of cancer patients. Our work thus provides a unique means to obtain viable and undamaged CTCs, which can subsequently be cultured. The results presented here offer unique pathways for better cancer diagnosis, prognosis, therapy monitoring, and metastasis research.

Author contributions: P.L., M.D., S.S., and T.J.H. designed research; P.L., Z.M., L.Z., Y.C., P.-H.H., and J.J.D. performed research; C.I.T. and J.J.D. collected patients' samples and provided clinical support; P.L., Z.M., Z.P., C.I.T., W.S.E.-D., M.D., S.S., and T.J.H. analyzed data; and P.L., Z.M., Z.P., C.I.T., W.S.E.-D., M.D., S.S., and T.J.H. wrote the paper.

Conflict of interest statement: P.L., Z.P., Y.C., M.D., S.S., and T.J.H. have filed a patent based on the work presented in this paper.

Freely available online through the PNAS open access option.

[1]Present address: Medical Oncology, Fox Chase Cancer Center, Philadelphia, PA 19111.

[2]To whom correspondence may be addressed. Email: mingdao@mit.edu, suresh@cmu.edu, or junhuang@psu.edu.

This article contains supporting information online at www.pnas.org/lookup/suppl/doi:10.1073/pnas.1504484112/-/DCSupplemental.

external acoustic radiation force, separation performance can be dynamically adjusted to accommodate the separation of different cell samples with distinct physical differences. In addition to size-based separation, acoustic-based separation also has the potential to differentiate cancer cells from normal cells based on their mechanical properties (13).

Although acoustic-based separation has been demonstrated for the successful separation of cultured cancer cells from WBCs (13, 14), it has not been applied so far to the separation of rare CTCs from clinical samples. This is mainly due to insufficient cell throughput and long-term operational instability in these devices. In this work, we report an optimized acoustic separation testing platform that is capable of enhancing separation throughput of cancer cells by up to 20 times compared with that previously achieved using tilted-angle standing surface acoustic waves (taSSAWs) while, at the same time, improving separation efficacy. We also apply the method to study blood samples obtained from cancer patients. Our device is built upon our recently developed taSSAW separation strategy (13). We performed systematic parametric studies of key factors influencing the performance of the testing platform and determined how these parameters affect the separation results. After optimizing the design parameters, such as the tilt angle and the length of the interdigitated transducers (IDTs) as well as the device power, we tested and validated the performance of the device by testing cultured cell lines for different types of cancer. As a result, the separation of rare cancer cells from WBCs was achieved with higher efficiency than previously possible. Finally, we applied our taSSAW device for high-throughput separation of clinical samples and successfully identified CTCs from breast cancer patients in all cases studied here.

Results

Working Principles and Optimization for High-Throughput Cell Separation. The taSSAW-based cell separation relies on the establishment of a standing acoustic wave field inside a fluidic microchannel. Particles present in such a flow channel will experience a primary acoustic radiation force:

$$F_a = -\left(\frac{\pi p_0^2 V_p \beta_w}{2\lambda}\right)\varphi(\beta,\rho)\sin(2ky), \qquad [1]$$

where p_0 and V_p are the acoustic pressure and the volume of the particle, respectively; λ and k are the wavelength and the wave number of the acoustic waves, respectively; and φ is the acoustic contrast factor, which is dependent on the compressibility (β) and density (ρ) of the particle and the liquid medium. The primary acoustic radiation force directs cells to either the pressure nodes or pressure antinodes depending on the sign of the acoustic contrast factor (φ). Mammalian cells in a PBS buffer or blood serum are pushed toward the pressure nodes. From Eq. **1**, it is seen that cells with different physical properties (i.e., size, density, and compressibility) experience different amplitudes of the primary acoustic radiation force, which enables the separation of these cells using acoustic waves.

Fig. 1*A* illustrates the process of cell separation in a taSSAW microfluidic device. As shown in Fig. 1*B*, a series of pressure nodes and pressure antinodes are established in a microfluidic channel at an angle tilted to the fluid flow direction. As a result, cells flowing through the microfluidic channels will pass multiple regions that have a pair of pressure nodes and antinodes. In each region, cells will experience different acoustic radiation forces (F_a) resulting in slightly different movement trajectories. By passing the cells through such regions repeatedly, the trajectory differences are further amplified, resulting in separation distances that can be from a few times to tens of times the acoustic wavelength, depending on the geometry of the channel. Thus, the taSSAW separation method (Fig. 1*C*) is able to overcome the limitation of conventional acoustic-based separation techniques, in which the total separation distance is limited to a quarter of the wavelength of the acoustic waves (15).

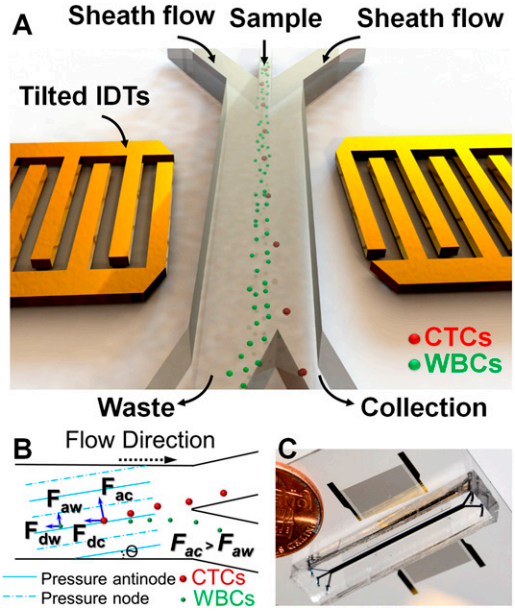

Fig. 1. Schematic illustration and image of the high-throughput taSSAW device for cancer cell separation. (*A*) Illustration of taSSAW-based cell separation. (*B*) Schematic of the working mechanism behind taSSAW-based cell separation. The direction of the pressure nodes and pressure antinodes were established at an angle of inclination (θ) to the fluid flow direction inside a microfluidic channel. Larger CTCs experience a larger acoustic radiation force (F_{ac}) than WBCs (F_{aw}). As a result, CTCs have a larger vertical displacement (normal to the flow direction) than WBCs. F_{dc} and F_{dw} are the drag force experienced by CTCs and WBCs, respectively. (*C*) An actual image of the taSSAW cell separation device. Blue ink was used to help visualize the microfluidic channel.

As demonstrated in our recent work (13), it is possible to use the taSSAW method to separate a cultured cancer cell line from WBCs under a relatively low sample flow rate of 1–2 μL/min. However, with this limited throughput, the previous taSSAW separation device could not be used to separate CTCs. Owing to the rareness of CTCs in a peripheral blood sample, it is necessary to process a large number of cells to detect the presence of tumor cells. Thus, high-throughput separation is a critical requirement for any separation method targeting clinical CTC applications. To apply taSSAW to the separation of CTCs, the throughput had to be improved significantly. In this regard we first performed a parametric study to determine the optimized design parameters such as the tilt angle and length of the IDTs, for high-throughput cell separation.

To find out the practical separation parameters for high-throughput cell separation, we first established a simulation model that can numerically describe particle trajectories in the taSSAW microfluidic device. The model considered the effects of the acoustic radiation force, the hydrodynamic drag force, and the laminar flow profile in the microchannel on separation performance. A detailed description of the simulation model can be found in *SI Text*, *Simulation Model of taSSAW-Based Separation*.

After calibrating the simulation model with 10-μm-diameter polystyrene (PS) beads (*SI Text* and Fig. S1), we first studied the dependence of separation distance on tilt angles under different flow rates. MCF-7 breast cancer cells and WBCs were used as the separation targets. The physical properties of these cells can be found in Table S1. The power input was set to 35 dBm. As shown in Fig. 2*A*, an optimum tilt angle for maximizing the separation distance can be found at each flow rate. The simulation results also indicate that as the flow rate increases, the tilt angle that achieves the highest separation distance decreases. The reason for this result may be attributed to the fact that smaller tilted angles allow longer traveling times between pressure antinodes and pressure nodes where the separation occurs. At high flow rates, the acoustic radiation force cannot dominate

over the drag force. In this situation, a longer separation time enabled by the smaller tilt angle will be more advantageous for cell separation. At lower flow rates, the separation distance between cells is no longer limited by their exposure time in the taSSAW because the acoustic radiation force is dominant over the drag force. In this case, larger tilt angles would increase the separation distance. For the same flow rate, the simulation indicated that the optimum separation angle increased as the power increased (Fig. S2). This is because at higher power the acoustic radiation force becomes more dominant. However, in practical situations, the applied power input cannot be too high because it could generate a level of Joule heating that could damage biological cells and/or device substrates.

Based on this parametric study, we identified the optimum tilt angle to achieve high-throughput cell separation. Under a practical power input (35 dBm), the separation distance for MCF-7 cells and WBCs at a 75 μL/min flow rate can reach ~600 μm with a tilt angle of ~5°, which is sufficient for successful separation at this throughput (Fig. 2*A*). When the gross flow rate is 75 μL/min, the sample flow rate can reach as high as 20 μL/min based on a 2.5:1 sheath-to-sample flow rate ratio, which means 1 mL of WBCs can be processed within 1 h using this design. Although higher total flow rates are also possible at even small tilt angles, the separation distance could be compromised, which is not desirable. It is important to keep the separation distance as large as possible to compensate for potential variations in experimental conditions.

After optimizing the flow rate, power input, and tilt angle, the remaining design parameter that needs to be optimized is the length of the IDTs (i.e., the length over which the SSAW is applied). As discussed above, the travel time of the cells across the taSSAW field, which is dependent on the length of IDTs, is critical to the cell-separation outcome. Therefore, the length of the IDTs would inevitably have an impact on the efficiency of cell separation. In general, the longer the time that it takes the cells to traverse the taSSAW field, the longer is the separation distance. However, the larger IDTs imply a lower energy density for the same power input, thereby decreasing the primary acoustic radiation force. There should thus be an optimum IDT length that can balance these two competing factors. To find the theoretical optimum IDT length, we used our simulation to study the relationship between the separation distance and the length of the IDTs at a fixed flow rate and power input. Fig. 2*B* shows that the separation distance reaches a maximum at around an IDT length of 8–10 mm. The decrease in the separation distance for shorter and longer IDTs lengths is caused by insufficient travel time through the taSSAW field and a lower energy density, respectively.

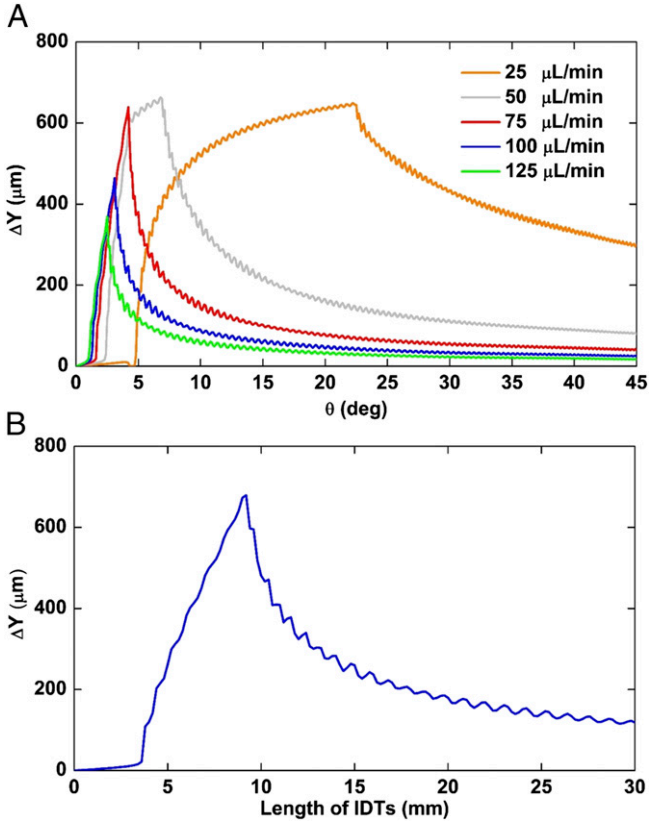

Fig. 2. Theoretical investigation of multiple design parameters for high-throughput separation using a taSSAW. (*A*) The relationship between tilt angle and separation distance under different flow rates. For higher flow rates, the optimum tilt angle becomes smaller. When flow rates are larger than 75 μL/min, the separation distance becomes smaller even at the optimum tilt angle. The power input is fixed at 35 dBm. (*B*) The relationship between the length of IDTs and the separation distance under a fixed power input (35 dBm) and flow rate (75 μL/min).

Demonstration of High-Throughput Separation of Cultured Cancer Cells from WBCs. We performed experimental verification of the high-throughput separation of cancer cells from WBCs based on the optimized values obtained from our simulation. We fabricated IDTs with a tilt angle of 5° and 10-mm length on a lithium niobate ($LiNbO_3$) piezoelectric substrate. A polydimethylsiloxane (PDMS) microfluidic channel with height and width of 110 μm and 800 μm, respectively, was bonded onto the substrate to form the separation device. For this, the input power is an important operating parameter. Higher input powers improve the recovery rate of cancer cells while reducing the removal rate of WBCs, leading to decreased separation purity. Therefore, it is necessary to obtain a profile of separation performance at different input powers. To evaluate the impact of varying the input power, the separation of MCF-7 and HeLa cells from WBCs was used as a model. To facilitate the characterization of device performance, we used an abundant number of cancer cells mixed with WBCs.

Fig. 3 *A* and *B* show the relationship between power inputs and cell-separation performance (the recovery rate and the removal rate of WBCs) for MCF-7 cells and for HeLa cells, respectively. Both MCF-7 cells and HeLa cells showed similar trends for power input dependence on separation performance. At lower input powers, the WBC removal rate could be maintained at ~99%, but the recovery rate for cancer cells was only 60–80%. Using a higher power input can result in greater than 90% cancer cell recovery and ~90% removal rate of WBCs. In particular, certain WBCs (e.g., monocytes) that have a larger size are more easily pushed by the acoustic field, resulting in a decrease in the WBC removal rate. The choice of the appropriate power input for cell separation thus depends on the outcome desired from optimization. If high sample purity is desired, a lower power input is preferred to ensure the highest removal rate of background cells. For CTC applications, the recovery rate of cancer cells is often more critical because of the inherent rarity of CTCs. For the following rare-cell separation experiments, we used the higher input power values (~37.5 dBm) to ensure a high recovery rate while maintaining ~90% removal rate of WBCs.

Fig. 4 shows cell separation in the taSSAW microfluidic device. Before applying the acoustic field, all of the cells flowed toward the waste outlet. Once the acoustic field was turned on, a clear separation between cancer cells and WBCs was visible. Cancer cells were directed toward the collection outlet, whereas a majority of WBCs still remained in the waste outlet (Movie S1). In summary, we experimentally demonstrated that the optimized taSSAW design is capable of separating cancer cells from WBCs with a flow rate of 1.2 mL/h, which allows us to study the separation performance of our device under rare-cell conditions.

Rare-Cell Separation with Multiple Cancer Cell Lines. After verifying that the device is capable of separating cancer cells from WBCs with a sample throughput of 1.2 mL/h, we investigated the recovery of rare cancer cells in a mixture of WBCs. We first examined the

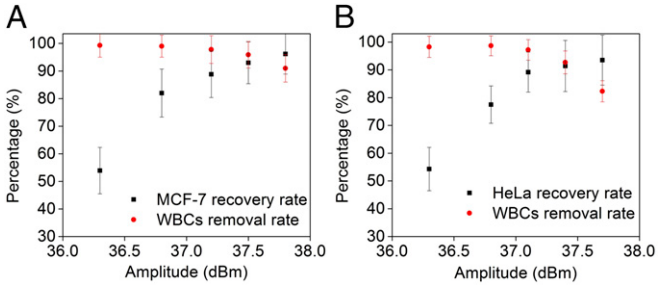

Fig. 3. The cancer cell separation performance under different power inputs at a 20 μL/min flow rate. (*A*) The relationship between power input and separation performance for separation of MCF-7 from WBCs. (*B*) The relationship between power input and separation performance for separation of HeLa from WBCs. Both cancer cell lines showed a similar relationship between the power input and separation performance. Higher power input would result in better cancer cell recovery rates and lower WBCs removal rates, and vice versa. Error bars represent the relative counting error. The number of cells (*n*) passing through collection channel and waste channel were counted, respectively. $n > 100$ for cancer cells, and $n > 350$ for WBCs.

separation performance of rare MCF-7 cells and also HeLa cells, because we used them to characterize the device performance, in a manner similar to that outlined in the previous section. The rare-cell population was simulated by spiking 50–1,000 calcein-AM–stained cancer cells into a 1-mL solution of WBCs. The concentration of WBCs is obtained by directly lysing 1 mL of human whole blood and resuspending the cells into 1 mL solution of PBS. The concentration ranges from 3–6 $\times$ 10^6 cells/mL. The cells were loaded into the taSSAW device at a flow rate of 1.2 mL/h for high-throughput separation. The power input was set at 37–38 dBm, and the input frequency was 19.573 MHz. Cells, from both the collection and waste outlets, were collected into two different Petri dishes with depth and height of 35 mm and 10 mm, respectively. The number of fluorescent cells in both collection and waste outlets was counted, and the recovery rate was obtained by dividing the number of cells in the collection channel by the number of total cells from both outlets. Typical images for both collection and waste outlets are shown in Fig. S3. The cell-counting results are summarized in Table 1. An average recovery rate greater than 87% was obtained for both the MCF-7 breast cancer cells and the HeLa cells.

After successfully demonstrating rare-cell separation with MCF-7 and HeLa cells, we also tested the high-throughput taSSAW device with other cancer cell lines. Because the physical properties of cells from real cancer patients are unknown a priori, it is important to test the tolerance of the device with different cell lines. For this purpose, we used melanoma and prostate cancer cell models, UACC903M-GFP cells and LNCaP cells, respectively. Unlike the previous separation for MCF-7 and HeLa cells in which we first optimized the separation parameters using abundant cell samples, we directly tested rare-cell concentrations of UACC903M-GFP cells and LNCaP cells using the same operating parameters to separate the MCF-7 and the HeLa cells. As shown in Table 1, a recovery rate greater than 83% for these cell lines was also obtained, indicating the robustness of the device for separating different cancer cell lines.

Study of Cell Viability and Proliferation After Acoustic Separation. As discussed above, the operating conditions of our taSSAW devices are conducive to preserving cell integrity during the cell separation process. To investigate the impact of current separation conditions on cell integrity, we examined both short-term viability and long-term cell proliferation following acoustic separation.

We first examined the short-term cell viability after taSSAW separation using a calcein-AM/propidium iodide (PI) staining method. One hundred microliters of HeLa cell solution (~1 $\times$ 10^6 cells/mL) was passed through the taSSAW separation device at a flow rate of 20 μL/min. The device-operating parameters were the same as those used in the aforementioned rare-cell-separation experiments. After running all of the samples through the device, cells from the collection outlet were stained with calcein-AM/PI for 15 min at room temperature to determine their viability. Cells with a calcein-AM+/PI− staining pattern were counted as live cells, whereas cells with calcein-AM−/PI+ and calcein-AM+/PI+ staining patterns were counted as dead cells. As shown in Fig. 5*A*, the cell viability of HeLa cells for the

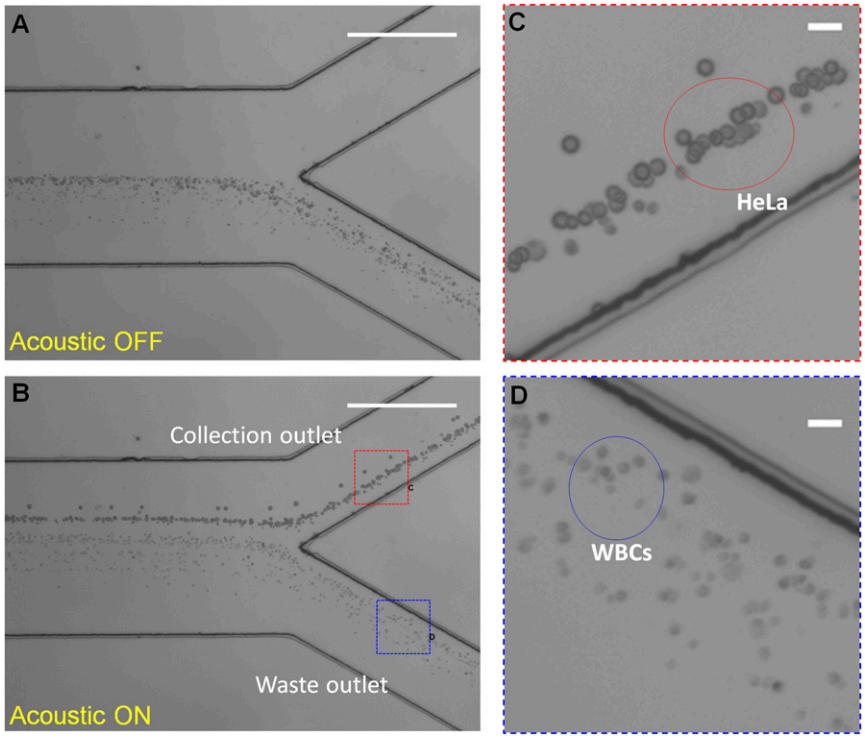

Fig. 4. Micrographs of the separation process with acoustic field ON and OFF. (*A*) The mixture of HeLa cells and WBCs through a microfluidic channel with the acoustic field OFF. All of the cells were directed to the lower waste outlet by the hydrodynamic flow. No separation is observed. (*B*) When the acoustic field is ON, larger HeLa cells were pushed to the collection outlet, whereas the smaller WBCs still remained in the waste outlet. The separation between HeLa cells and WBCs can be observed. The stacked images are from 50 consecutive frames. (Scale bars, 515 μm.) (*C* and *D*) Zoomed-in images of the collection outlet and the waste outlet, respectively. (Scale bars, 30 μm.)

acoustic ON and OFF groups were determined to be 90.4 ± 4.7% and 91.5 ± 7.6%, respectively. The results indicated no significant change in cell viability after applying the taSSAW. Representative fluorescence images are shown in Fig. 5 *B* and *C*.

After determining short-term cell viability, it is also important to examine whether cells continue to proliferate normally after the separation process. To simulate the actual CTC separation conditions, 100 HeLa cells were spiked into 1 mL of PBS solution and passed through the acoustic device. The flow rate and acoustic power input were the same as previous rare-cell separation experiments. The separated HeLa cells were collected into a 35- ×10-mm Petri dish with 1 mL of DMEM/F12 cell culture medium. After collecting cells for about 1 h, the cell-collection Petri dish was transferred to an incubator. Cells were then cultured overnight at 37 °C and under 5% CO_2. After culturing for 12 h, the 50% diluted DMEM/F12 cell culture medium (vol/vol, PBS/medium) was changed to the original undiluted medium. Fig. 5*D* shows images of the cultured HeLa cells focused at the same location over a long time period (1 wk). Normally, HeLa cells divide once every 20 h. From the images, we see that the cells have maintained their normal proliferation rates after running through the taSSAW separation conditions. Collectively, these short-term and long-term cell viability and proliferation experiments demonstrated that our high-throughput taSSAW separation approach is biocompatible and can maintain long-term, normal cell physiological processes.

Probing CTCs from Breast Cancer Patient Blood Samples. As a practical demonstration, we tested our taSSAW device with blood samples obtained from three patients with metastatic breast cancer. Immunofluorescent staining of cytokeratin (CK) and pan-leukocyte marker CD45 was used to first determine the identity of the cells using conventional detection methods. Cells were identified as CTCs if the immunofluorescent pattern is DAPI+/CK8,18+/CD45−; otherwise, cells were identified as WBCs. Based on this immunostaining detection criteria and using the taSSAW devices, 59 and 8 CTCs were found in the first two patients, respectively, in 2-mL blood samples from each patient. Both of these patients had CTCs detected by the Veridex assay on previous occasions. The third patient had only one CTC after screening 6 mL of blood. Typical fluorescent images are shown in Fig. 6. WBCs can be distinguished from the CTCs because they showed an immunostaining pattern of DAPI+/CK8,18−/CD45+. Using immunofluorescence, we could also check the expression of certain protein markers in patients' CTCs after our taSSAW-based separation. In this case, we examined the expression of estrogen receptor (ER) in the patients' CTCs. As shown in Fig. 6*A*, the MCF-7 cell line was used as a positive control for ER. Compared with the fluorescent signal from the ER in the MCF-7 cells, all of the patient samples were considered negative for ER. All three patients had initial diagnosis of ER+ breast cancer. The first two patients (with CTC counts of 59 and 8, respectively) had been heavily pretreated with multiple lines of endocrine therapy as well as chemotherapy and had chemotherapy refractory disease. In the first patient immunohistochemical staining of a biopsy of a metastatic site (bone)

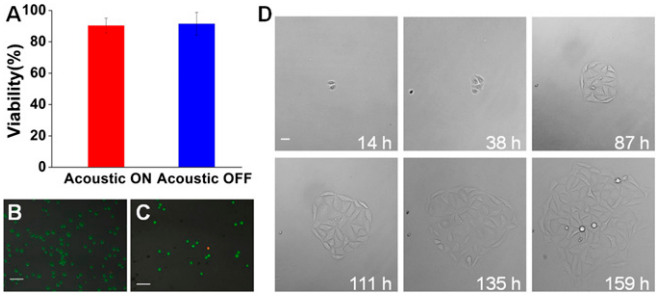

Fig. 5. Short-term viability test and long-term culture of HeLa cells after taSSAW separation. (*A*) Cell viability comparison between the acoustic ON group and acoustic OFF group using calcein-AM/PI staining method. No significant difference was found between the "Acoustic ON" group and control group. (*B* and *C*) Representative images of live/dead cell staining for the "Acoustic ON" group and the control group, respectively. Calcein-AM, PI, and bright-field channels were overlaid and pseudo colors were assigned to calcein-AM (green) and PI (red) channels. Red color indicates dead cells. (Scale bars, 100 μm.) (*D*) Long-term culture of rare HeLa cells after acoustic separation. (Scale bar, 35 μm.)

showed persistent ER positivity and progesterone receptor (PR) positivity at 5%; the second patient had biopsy of her metastatic tumor in the pelvis and this was ER-positive at 100% and PR-positive at 1%. Loss of ER positivity in the CTCs from patients with initial diagnosis of ER positive breast cancer has been previously reported and could be a reflection of tumor heterogeneity (16). The third patient had a low (1) CTC count, which is consistent with the fact that the blood was drawn within 2 mo after initiating a new line of endocrine therapy to which she responded; this was ascertained by clinical examination and imaging (CT scans).

Discussion

In this work, we demonstrated taSSAW-based high-throughput cell separation by systematically investigating the effects of multiple design parameters on the separation performance. We showed that under different flow rates the optimum tilt angle would be different. In general, higher flow rates would require smaller optimum tilt angles. After systematic optimization, we demonstrated that the taSSAW device was capable of separating cancer cells from WBCs under a flow rate of 20 μL/min. This result facilitated the practical use of this device to isolate rare cells from spiked blood samples. We further demonstrated that this high-throughput cell separation method works with real clinical samples by successfully isolating CTCs in the blood samples from three breast cancer patients. The acoustic-based separation method demonstrated here features several advantages for CTC separation applications such as high biocompatibility, automated operation, and label-free, contactless nature, all in a simple, inexpensive and compact device.

The taSSAW-based separation involves multiple parameters that may affect the cell-separation performance, such as the flow

Table 1. Rare-cell separation with multiple-spiked cancer cell lines

Cell line	Cells ratio (cancer cells/WBCs)	No. of cancer cells (collection outlet)	No. of cancer cells (waste outlet)	Recovery rate, %
MCF-7	1:40,000	121	20	86
MCF-7	1:40,000	90	11	89
MCF-7	1:40,000	52	2	96
HeLa	1:6,000	907	165	85
HeLa	1:100,000	49	10	83
HeLa	1:40,000	131	7	95
UACC903M-GFP	1:100,000	64	12	84
UACC903M-GFP	1:100,000	36	7	84
UACC903M-GFP	1:100,000	28	5	85
LNCaP	1:20,000	111	12	90

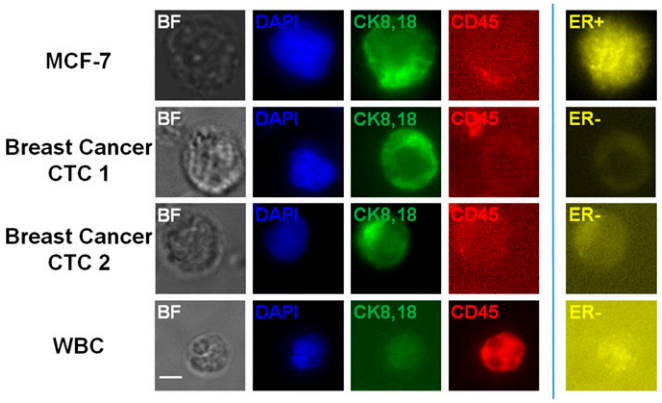

Fig. 6. Immunofluorescence images for the identification of CTCs in blood samples from breast cancer patients. Four channels, DAPI, CK8,18, CD45, and ER, were examined. The MCF-7 cell was used as the positive control, showing a staining pattern of DAPI+/CK8,18+/CD45−/ER+. CTCs were identified as they showed a staining pattern DAPI+/CK8,18+/CD45−. In contrast, WBCs showed a staining pattern DAPI+/CK8,18−/CD45+. (Scale bar, 4 μm.)

rate, input power, tilt angle, and the length of the IDTs, in addition to cell physical properties. All these parameters have interdependent and complex relationships. Therefore, it would require a large combination of experimental trials to determine the optimized values. In this work, we have shown that a straightforward simulation model that carefully considered the acoustic radiation force, the hydrodynamic drag force, channel flow with a laminar velocity profile, and cell physical properties could effectively guide the optimization of the taSSAW device for high-throughput cell separation. The simulation model can be further improved if the physical properties of clinical CTC samples were readily available. However, the current physical properties of clinical CTCs, specifically compressibility, are still largely undocumented and unknown. In future studies, it will be ideal to establish the physical and mechanical property profiles of CTCs from different cancer populations (17). By establishing a statistical database of the physical properties of CTCs from patient samples, the current simulation model can be further refined, thereby leading to more optimized taSSAW designs for clinical CTC samples. Conversely, it could also enable probing the mechanical properties of CTCs via acoustic methods.

In our previous publication (13), we demonstrated that the taSSAW method could effectively separate particles with small difference in physical properties such as size, density, and compressibility. For example, we separated 9.9-μm PS beads from 7.3-μm ones, with an efficiency of 97% or higher. In this work, we demonstrated the effective separation of rare cancer cells (with average diameters of 16 or 20 μm depending on the cancer cell lines used) from WBCs (diameter ∼12 μm). Cancer cell recovery rate is >83% (83–96%) and WBC removal rate is ∼90%. The method is expected to work very well for cancer cells that have significant size (or density/compressibility) differences with respect to WBCs. For cancer cells that have similar physical properties compared with WBCs, the method could be less effective and optimized specific device design would be even more critical in that case.

In this work, RBCs were removed using an RBC lysis buffer to facilitate the separation process. The use of an RBC lysis buffer has also been used by other CTC separation methods and has shown no negative impact on cancer cells (8). However, the RBC lysis step added extra sample processing time and decreased the overall processing throughput. In future studies, it would be desirable to integrate an RBC-removal function into the same microfluidic chip. For instance, continuous-flow RBC removal methods predicated upon deterministic later displacement could be integrated with the taSSAW-based separation device to enable processing of whole blood (18).

Although this work focuses on developing taSSAW for high-throughput separation of CTCs, this approach is not limited to CTC applications. Virtually all separation applications will benefit from an increase in throughput. Acoustic-based separation has been demonstrated in many applications where the physical properties of target cells are different from those of the background cells (19, 20). Therefore, the high-throughput taSSAW approach developed here could also improve separation performance in other applications, such as cell washing, cell synchronization, blood component separations, and bacteria separation.

Materials and Methods

Device Fabrication and Experimental Setup. Details of the device fabrication process flow can be found in our previous work (13). Details of the experimental setups and procedures can be found in *SI Text, Experimental Setup and Procedures*.

Cell Culture and Sample Preparation. Standard cell culture and handling procedures were followed. Detailed procedures can be found in *SI Text, Cell Cultures and Sample Preparation*.

Patient Blood Processing and Image Acquisition. Informed consent was obtained for clinical samples used on a clinical protocol approved by The Pennsylvania State University Institutional Review Board. Detailed procedures of blood processing, immunofluorescence staining, and image acquisition can be found in *SI Text, Patients' Blood Processing, Immunofluorescence Staining, and Image Acquisition*.

ACKNOWLEDGMENTS. We thank Mr. Joseph Rufo for manuscript editing. We gratefully acknowledge financial support from NIH Grants 1 R01 GM112048-01A1 and 1R33EB019785-01, the National Science Foundation, and the Penn State Center for Nanoscale Science (Materials Research Science and Engineering Center) under Grant DMR-0820404. Z.P. and M.D. also acknowledge partial support from NIH Grant U01HL114476.

1. Plaks V, Koopman CD, Werb Z (2013) Cancer. Circulating tumor cells. *Science* 341(6151):1186–1188.
2. Yu M, et al. (2014) Cancer therapy. Ex vivo culture of circulating breast tumor cells for individualized testing of drug susceptibility. *Science* 345(6193):216–220.
3. Hou J-M, et al. (2011) Circulating tumor cells as a window on metastasis biology in lung cancer. *Am J Pathol* 178(3):989–996.
4. Li P, Stratton ZS, Dao M, Ritz J, Huang TJ (2013) Probing circulating tumor cells in microfluidics. *Lab Chip* 13(4):602–609.
5. Nagrath S, et al. (2007) Isolation of rare circulating tumour cells in cancer patients by microchip technology. *Nature* 450(7173):1235–1239.
6. Hoshino K, et al. (2011) Microchip-based immunomagnetic detection of circulating tumor cells. *Lab Chip* 11(20):3449–3457.
7. Suresh S (2007) Biomechanics and biophysics of cancer cells. *Acta Biomater* 3(4):413–438.
8. Warkiani ME, et al. (2014) An ultra-high-throughput spiral microfluidic biochip for the enrichment of circulating tumor cells. *Analyst (Lond)* 139(13):3245–3255.
9. Zheng S, et al. (2011) 3D microfilter device for viable circulating tumor cell (CTC) enrichment from blood. *Biomed Microdevices* 13(1):203–213.
10. Gupta V, et al. (2012) ApoStream(™), a new dielectrophoretic device for antibody independent isolation and recovery of viable cancer cells from blood. *Biomicrofluidics* 6(2):24133.
11. Lin BK, McFaul SM, Jin C, Black PC, Ma H (2013) Highly selective biomechanical separation of cancer cells from leukocytes using microfluidic ratchets and hydrodynamic concentrator. *Biomicrofluidics* 7(3):34114.
12. Ding X, et al. (2013) Surface acoustic wave microfluidics. *Lab Chip* 13(18):3626–3649.
13. Ding X, et al. (2014) Cell separation using tilted-angle standing surface acoustic waves. *Proc Natl Acad Sci USA* 111(36):12992–12997.
14. Augustsson P, Magnusson C, Nordin M, Lilja H, Laurell T (2012) Microfluidic, label-free enrichment of prostate cancer cells in blood based on acoustophoresis. *Anal Chem* 84(18):7954–7962.
15. Petersson F, Åberg L, Swärd-Nilsson A-M, Laurell T (2007) Free flow acoustophoresis: Microfluidic-based mode of particle and cell separation. *Anal Chem* 79(14):5117–5123.
16. Babayan A, et al. (2013) Heterogeneity of estrogen receptor expression in circulating tumor cells from metastatic breast cancer patients. *PLoS ONE* 8(9):e75038.
17. Bao G, Suresh S (2003) Cell and molecular mechanics of biological materials. *Nat Mater* 2(11):715–725.
18. Ozkumur E, et al. (2013) Inertial focusing for tumor antigen-dependent and -independent sorting of rare circulating tumor cells. *Sci Transl Med* 5(179):179ra147.
19. Chen Y, et al. (2014) Rare cell isolation and analysis in microfluidics. *Lab Chip* 14(4):626–645.
20. Lenshof A, Laurell T (2010) Continuous separation of cells and particles in microfluidic systems. *Chem Soc Rev* 39(3):1203–1217.

Supporting Information

Li et al. 10.1073/pnas.1504484112

SI Text

Simulation Model of taSSAW-Based Separation. The detailed physical model of the simulation in this work was described in our previous work (1). Briefly, to simulate the trajectories of solid particles, we considered the effects of primary acoustic radiation force, drag force, and the flow profile in a rectangular microfluidic channel. The primary acoustic radiation force is described as

$$F_a = -\left(\frac{\pi p_0^2 V_p \beta_w}{2\lambda}\right)\varphi(\beta,\rho)\sin(2ky), \quad [S1]$$

$$\varphi(\beta,\rho) = \frac{5\rho_P - 2\rho_m}{2\rho_p + \rho_m} - \frac{\beta_p}{\beta_m}, \quad [S2]$$

where p_0, λ, V_p, ρ_p, ρ_m, β_m, β_p, μ, and R_p are the acoustic pressure, acoustic wavelength, volume of particle, density of the particle, density of medium, compressibility of the medium, compressibility of the particle, viscosity of the medium, and radius of the particle, respectively.

The drag force is described as

$$F_d = -6\pi\mu R_p u_r, \quad [S3]$$

where u_r is the relative velocity of the particle. The velocity profile of laminar flow in a rectangular channel (with width a and height b) is described as

$$u_f = \frac{\nabla P}{4\mu}\left[1 - \frac{Z^2}{b^2} + 4\sum_{n=1}^{\infty}\frac{(-1)^n}{\alpha_n^3}\frac{\cosh\left(\alpha_n\frac{Y}{b}\right)}{\cosh\left(\alpha_n\frac{a}{b}\right)}\cos\left(\alpha_n\frac{z}{b}\right)\right], \quad [S4]$$

where Z is the coordinate in the channel height direction, and Y is the coordinate in the width direction, ∇P is the pressure gradient, and $\alpha_n = (n - (1/2))\pi$. Based on these basic equations, a customized MATLAB (The MathWorks, Inc.) code was developed to simulate and depict the movement of particles inside the microfluidic channels.

In the simulation, the dimensions of the channel were 10,000 μm (length) × 800 μm (width) × 112 μm (height). The phase velocity of SAW is 3,997 m/s. The frequency of the SAW was ∼19.6 Mhz. The default wavelength of SAW was 200 μm. The default angle of inclination for beads calibration was θ = 4.8°. For the liquid medium of water, the compressibility is 4.6×10^{-10} Pa^{-1} and its density is 997 kg/m^3. The viscosity of water at room temperature is 0.001 Pa·s. The compressibility of PS beads is 2.16×10^{-10} Pa^{-1}, and the density of PS beads is 1,050 kg/m^3. The density of $LiNbO_3$ substrate is 4,650 kg/m^3. In our experiments, the variation in the initial position of PS beads was 20–30 μm in the direction of the channel width; as a result, in our simulations, we considered a variation of 30 μm for the initial position of PS beads. The acoustic pressure was estimated by $p_0 = \sqrt{\alpha P_I \rho_s c_s / A_w}$, where P_I is the input power to the IDTs, ρ_s and c_s are the density of the $LiNbO_3$ substrate and the phase velocity of SAW, respectively, A_w is the working area evaluated as the channel length multiplied by the distance between the two IDTs (10,000 ×16,000 μm in this work), and α is the defined as the power conversion efficiency. The parameter α was calibrated by comparing the simulated trajectories of PS beads with the ones obtained in experiments. Its value was calibrated to be ∼0.15 for the device used in our experiments.

Experimental Setup and Procedures. The taSSAW microfluidic device was placed on a stage of an inverted microscope during the separation experiment. The fluid flow, including sheath fluid and sample fluid, was controlled by individual syringe pumps (neMESYS; Centoni GmbH). The microfluidic device and syringe pumps were connected by polythene tubing (Smith Medical International) with an inner diameter of 0.28 mm. Before each experiment, isopropanol (VWR) was flushed through the whole microfluidic device to remove all of the air bubbles in the channel followed by 1× PBS (Life Technologies) washing for 30 min. The sample mixture was then introduced to the device at a flow rate of 20 μL/min. Cells from the device outlets were collected either in a 35- ×10-mm Petri dish (Corning) or 1.7-mL Eppendorf centrifuge tubes. The taSSAW was established by applying an rf signal to the IDTs on the $LiNbO_3$ substrate. The rf signal was generated by a function generator (E4422B; Agilent) and an amplifier (25A100A; Amplifier Research). The frequency was set at 19.573 MHz, and the power inputs ranged from 34 to 39 dBm.

Cell Cultures and Sample Preparation. MCF-7 (HTB-22) and HeLa (CCL-2) cells were purchased from ATCC. MCF-7 cells were cultured with Earle's minimum essential medium (Cellgro; Corning) supplemented with 10% (vol/vol) FBS solution (Atlanta Biologicals) and 1% penicillin–streptomycin solution (Mediatech). HeLa cells were cultured with DMEM/Ham's F-12 50/50 Mix (Life Technologies) supplemented with 10% (vol/vol) FBS and 1% penicillin–streptomycin solution. Both of the cell lines were maintained in an incubator (NU-4750; NuAire) with a temperature of 37 °C and 5% CO_2 level. Before each experiment, cells were detached from the surface of culture flasks by 0.05% trypsin (Cellgro; Corning). The resulting cell suspensions were then centrifuged at 118 × g and resuspended with 1× PBS buffer. To label cells with calcein-AM (Invitrogen), cells were incubated with 1 μM calcein-AM in 1× PBS solution at room temperature for 15 min. Cells were washed by spinning down at 118 × g and resuspending into a new portion of PBS solution. To prepare WBCs, human whole blood (Zen-Bio) was lysed with RBC lysis buffer (eBioscience) with a volume ratio of 1:10. The mixture solution was incubated for 5–10 min at room temperature and then centrifuged at 800 × g. The supernatant was removed and the cell pellet was resuspended using PBS. For long-term storage, WBCs were fixed using 4% (wt/vol) paraformaldehyde (ChemCruz) at room temperature for 30 min.

Patients' Blood Processing, Immunofluorescence Staining, and Image Acquisition. Within 24 h of collection, blood cells were first lysed using RBC lysis buffer for 5 min to remove the majority of erythrocytes. WBCs were collected by centrifuging the blood solution at 800 × g and resuspended in the same volume as the whole blood in 1× PBS solution with 0.1% PF-68. Then the sample was run through the taSSAW device at a flow rate of 1.2 mL/h. The sample was then taken from the collection outlet and concentrated into one 1.7-mL centrifuge tube for immunofluorescence staining.

For immunofluorescence staining, cells were first fixed using 4% (wt/vol) paraformaldehyde (ChemCruz) for 10 min at room temperature and permealized by 0.1% Triton X-100 (Sigma) in PBS solution for 10 min at room temperature. Cells were then blocked by 200 μL of 3% (wt/vol) BSA in PBS solution (Life Technologies) for 30 min. After blocking nonspecific binding sites, 5 μL FITC-labeled mouse anti-CK 8, 18 (Abcam), 1 μL rabbit anti-ER (CellSignal), and 5μL Cy5-labeled mouse anti-CD45

(eBioscience) were added into the 3% (wt/vol) BSA solution and incubated at 4 °C overnight. After overnight incubation, cells were washed with PBS and stained with 5 μL PE-labeled anti-rabbit IgG (Life Technologies) for 2 h at room temperature. Before transporting cells to a chamber slide for observation, DAPI was added to the cell solution for nuclei staining.

Both bright-field and fluorescence images were obtained using an inverted epifluorescence microscope (Ti-U Eclipse; Nikon) and a CCD camera (CoolSNAP HQ^2; Photometrics); 4× (0.10 N.A.), 10× (0.30 N.A.), 20× (0.45 N.A.), and 60× (0.85 N.A.) objectives were used in the experiment. For the CTC counting experiment, the whole chamber slide was scanned manually with a 20× objective. For CTC imaging under the 60× objective, the cell samples were transferred to a customized PDMS chamber with a no. 1 glass slide as the bottom. All of the microscopy images were processed and analyzed using ImageJ (NIH).

1. Ding X, et al. (2014) Cell separation using tilted-angle standing surface acoustic waves. *Proc Natl Acad Sci USA* 111(36):12992–12997.

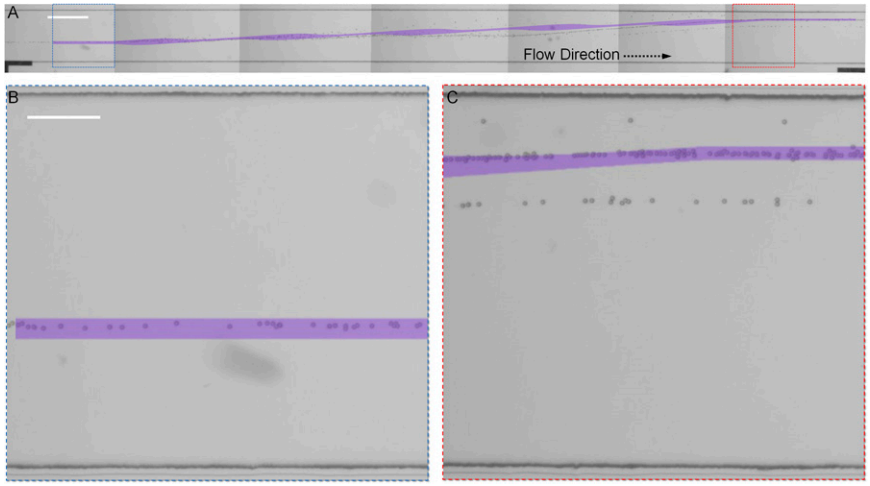

Fig. S1. (*A*) The experimental and simulation trajectories of 10-μm PS particles in the taSSAW separation device. The transparent purple line is calculated from the simulation model. (Scale bar, 650 μm.) (*B* and *C*) Enlarged images showing the match between the simulation trajectory and the main experimental trajectory at upstream and downstream locations in the taSSAW field, respectively. The power input was 38 dBm; flow rate was 170 μL/min; IDTs length was 10 mm. (Scale bar, 160 μm.)

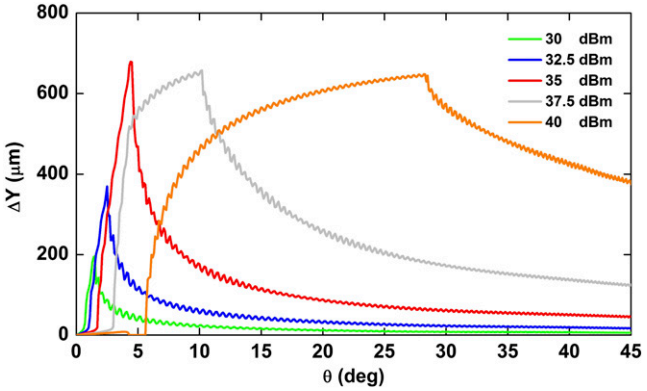

Fig. S2. The relation between tilted angle and separation distance under different power inputs. To reach the same separation distance, smaller tilted angles required much less power input. The flow rate is fixed at 75 μL/min.

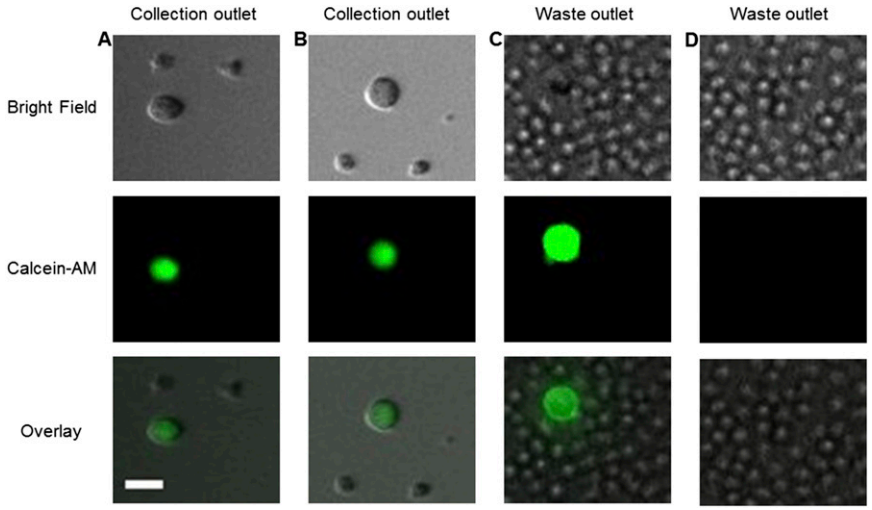

Fig. S3. Micrographs of HeLa cells and WBCs after the taSSAW-based rare-cell separation. (*A* and *B*) Images of HeLa cells and WBCs that were found in the collection outlet. HeLa cells were stained with calcein-AM dye. (*C* and *D*) Images of HeLa cells and WBCs that were found in the waste outlet. Although some HeLa cells can also be found in the waste outlet (<15%), the concentration of background WBCs were much higher. (Scale bar, 23 μm.)

Table S1. Physical properties of cells used for taSSAW separation

Cell line	Average diameter, μm	Density, g/cm^3	Compressibility (×10^{-10} Pa^{-1})
MCF-7	20	1.068 (1)	4.22 (1)
HeLa	16	1.0357 (2)	3.55 (3, 4)
UACC903M-GFP	20	N/A	N/A
LNCaP	20	N/A	N/A
WBCs	12	1.019 (5)	3.99 (5)

N/A, not available.

1. Hartono D, et al. (2011) On-chip measurements of cell compressibility via acoustic radiation. *Lab Chip* 11(23):4072–4080.
2. Czerlinski G, et al. (1987) Determination of the density of cells from sedimentation studies at 1G. *J Biol Phys* 15(2):29–32.
3. Tomankova K, Kolar P, Malohlava J, Kolarova H (2012) Mechanical characterisation of HeLa cells using atomic force microscopy. *Current Microscopy Contributions to Advances in Science and Technology*, ed Mendez-Vilas A (Formatex Research Center, Badajoz, Spain), pp 549–554.
4. Guigas G, Kalla C, Weiss M (2007) The degree of macromolecular crowding in the cytoplasm and nucleoplasm of mammalian cells is conserved. *FEBS Lett* 581(26):5094–5098.
5. Ding X, et al. (2014) Cell separation using tilted-angle standing surface acoustic waves. *Proc Natl Acad Sci USA* 111(36):12992–12997.

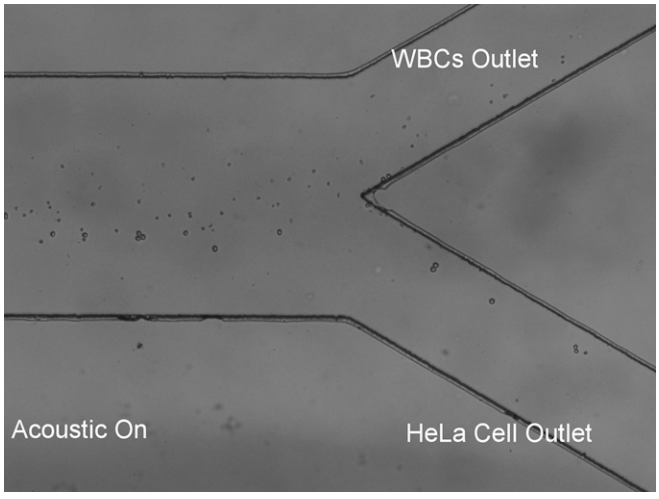

Movie S1. Separation of HeLa cells from WBCs.

Movie S1